ACS OMEGA

Open Access

http://pubs.acs.org/journal/acsodf

Article

Surface Plasmon Field-Enhanced Raman Scattering Co-Excited by P-Polarized and S-Polarized Light Based on Waveguide-Coupled Surface Plasmon Resonance Configuration

Yu Liu, Jingqiu Liang, Shuping Xu, and Yijia Geng*

Cite This: *ACS Omega* 2023, 8, 41953−41959

Read Online

ACCESS | Metrics & More | Article Recommendations | Supporting Information

ABSTRACT: We constructed a waveguide-coupled surface plasmon resonance (WCSPR) structure to enhance Raman scattering. In this structure, P-polarized and S-polarized incident lasers can simultaneously coexcite the evanescent field, thereby further enhancing Raman scattering. This configuration is a five-phase Kretschmann resonance setup that consists of a SF10 prism/inner Ag film/SiO_2 film/outer Ag film/water structure. The WCSPR configuration effectively concentrates and confines the evanescent field excited by the incident light. Ag nanoparticles assembled on the outer Ag film surface enhance the evanescent field further by means of surface plasmon resonance. By finely tuning the thickness of the Ag and SiO_2 films, it is possible to achieve a coincidence between the SPR angle of P-polarized light and that of S-polarized light. At this angle, both P- and S-polarized light can jointly elevate the evanescent field intensity, leading to the simultaneous enhancement of the electric fields at the upper, lower, left, and right parts of the silver nanoparticles and generating maximum evanescent field enhancement. We achieved an electric field enhancement of up to 10^3 around the nanoparticles, leading to more SERS hotspots and comparable SERS enhancement capability to gap-type hotspots. Our WCSPR structure combined with the nanoparticles offers a feasible strategy for the SERS detection of large molecules that cannot be placed in traditional gap-type hotspots. It is highly convenient for SERS detection of large molecules.

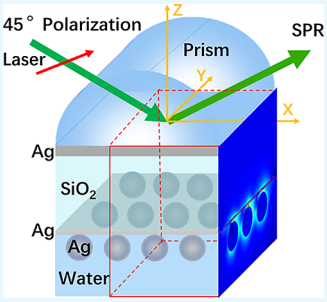

INTRODUCTION

Raman spectroscopy is a crucial technique for nondestructive, nonlabel analysis of molecular structures and has a wide range of applications in fields such as food safety, medical health, and contraband inspection.[1−7] However, a serious disadvantage of Raman spectroscopy is the weak signal, which limits its development and application.[8] The discovery of the surface-enhanced Raman scattering (SERS) phenomenon has greatly improved the signal intensity of Raman spectroscopy and expanded the application field of Raman spectroscopy.[3,9−13] SERS has two enhancement mechanisms: an electromagnetic enhancement mechanism and a chemical enhancement mechanism.[14] Based on the electromagnetic enhancement mechanism, researchers have developed various SERS substrates, such as nanoparticles and periodic nanostructures, to improve detection sensitivity and signal uniformity.[15−17] However, these structures are complicated, expensive, and difficult to manufacture in large areas. As a result, researchers are actively exploring the development of low-cost, easily reproducible SERS substrates in large areas.[18,19]

Surface plasmon resonance (SPR) is an important part of the SERS electromagnetic enhancement mechanism.[20,21] It can significantly increase the electric field intensity of incident light near the SPR resonance angle, resulting in an enhanced SERS signal.[22−24] SERS substrates based on SPR structures only require vapor-depositing one or several layers of dielectric film and are easy to manufacture and prepare in a large area. There are four types of SPR structures: traditional SPR,[25,26] long-range SPR,[27−29] CWSPs,[30,31] and WCSPR structures.[32,33] All four types of structures can be used for enhancing Raman scattering.

Traditional and long-range SPR structures only allow for excitation of the SPR via P-polarized light. However, the CWSPs and WCSPR structures enable both P and S polarizations to excite surface plasmons and enhance Raman scattering. When nanoparticles are adsorbed onto the SPR structure and excited by P-polarized light, the electric field at the upper and lower portions of the nanoparticles is greatly enhanced.[34] On the other hand, when excited by S-polarized light, the electric fields on the left and right sides of the nanoparticles are enhanced instead.[35] Xu et al. have successfully used P-polarized light to increase the electric field between nanoparticles and a silver film under the LRSPR structure, which they then used to enhance Raman scattering.[20] They have also employed a combination of CWSP structure and nanoparticles to enhance the electric field on the sides of the nanoparticles under the excitation of S-

Received: September 19, 2023
Accepted: October 5, 2023
Published: October 23, 2023

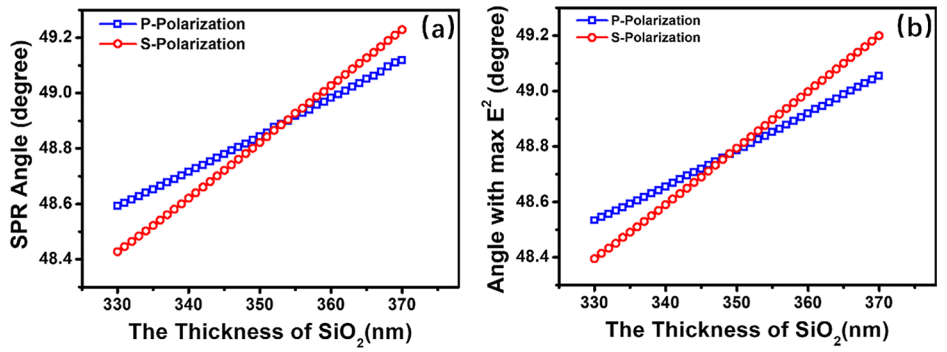

Figure 1. (a) Variation of surface plasmon resonance angle with SiO_2 thickness for P-polarization incident laser [□ (blue)] and S-polarization incident laser [○ (red)]; (b) variation of angle corresponding to maximum field enhancement with SiO_2 thickness for P-polarized incident laser [□ (blue)] and S-polarized incident laser [○ (red)].

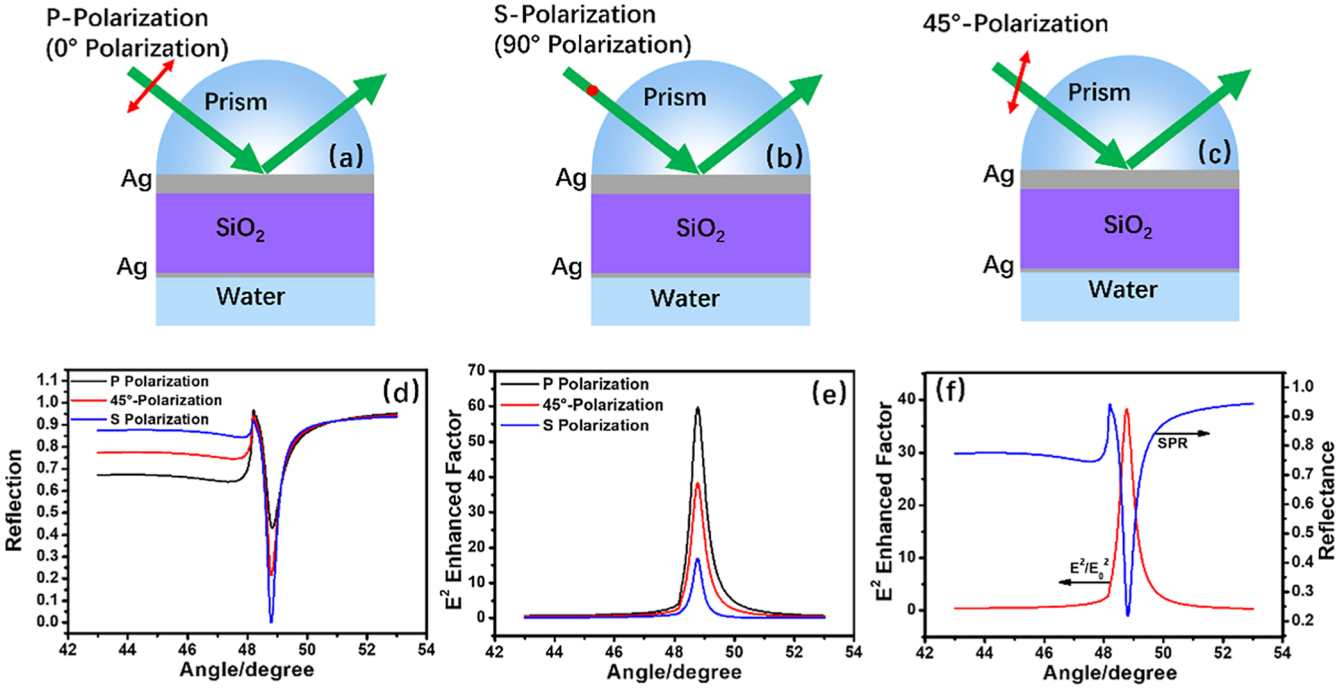

Figure 2. Schematic diagrams of the Kretschmann prism-coupling WCSPR structure with P-polarization incident laser (a), S-polarization incident laser (b), and 45°-polarization incident laser (c); (d) SPR curve simulation for the WCSPR structure based on P-polarization laser, S-polarization laser, and 45°-polarization laser; (e) angular electric field scan simulation for the WCSPR structure based on P-polarization laser, S-polarization laser, and 45°-polarization laser; (f) SPR curve and angular electric field scan simulation for the WCSPR structure based on 45°-polarization laser. The WCSPR structure was a five-layer resonance structure composed of a prism (n = 1.79)/25 nm inner silver film/349 nm SiO2 film (n = 1.46)/5 nm outer silver film/water layer.

polarized light.[32] If the electric fields of nanoparticles in the upper, lower, left, and right directions can be enhanced simultaneously, then it will increase the number of SERS hot spots and further enhance the Raman scattering signal. Moreover, by positioning larger biomolecules between nanoparticles, we can detect those biomolecules that cannot be placed between nanoparticles and silver films. However, due to the different resonance angles of excitation between P- and S-polarization, simultaneous enhancement of the upper, lower, left, and right electric fields of nanoparticles to create more hot spots has been challenging.

In this study, a 5-layer WCSPR structure consisting of a prism, an inner layer of silver, a layer of SiO_2, an outer layer of silver, and water was constructed. The thicknesses of the silver and SiO_2 films were adjusted to match the SPR resonance angle under P-polarized laser excitation with the SPR resonance angle under S-polarized laser excitation. At a specific angle, the SPR resonance angle under P-polarized laser excitation aligns with the SPR resonance angle under S-polarized laser excitation. This adjustment is crucial for ensuring the simultaneous enhancement and extinction of the field intensity for both P-polarized light and S-polarized light within the structure. In this structure, any polarization state of light can excite the surface plasmon field and enhance the Raman signal; therefore, it is not necessary to specifically adjust the incident light to P-polarized light. Next, silver nanoparticles are absorbed onto the surface of the WCSPR structure and then excited by a 45° polarized laser at the resonance angle to generate surface plasmons (SPs). Since the 45° polarized laser contains both P-polarized and S-polarized components, it can simultaneously enhance the electric field of the silver nanoparticles on the top, bottom, left, and right sides,

https://doi.org/10.1021/acsomega.3c06740
ACS Omega 2023, 8, 41953−41959

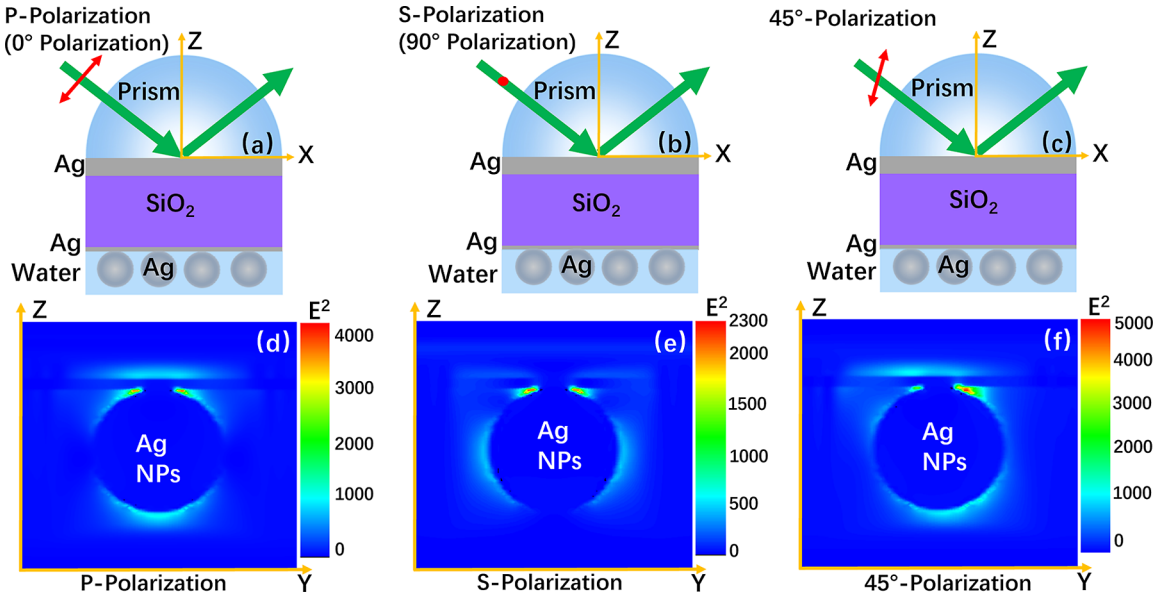

Figure 3. Schematic diagrams of silver nanoparticles adsorbed on the WCSPR structure with P-polarization incident laser excitation (a), S-polarization incident laser excitation (b), and 45°-polarization incident laser excitation (c); electric field distributions around the silver nanoparticles adsorbed on the WCSPR structure with the excited P-polarization incident laser (d), S-polarization incident laser (e), and 45°-polarization incident laser (f). The WCSPR structure for FDTD simulation was a five-layer structure composed of prism (n = 1.79)/25 nm silver film/349 nm SiO2 film (n = 1.46)/5 nm outer silver film/water layer. The diameter of the silver nanoparticle is 60 nm. The incident angle is 48.77°, which is the resonance angle.

generating more SERS hotspots. Additionally, by adjusting the polarization direction of the incident light, the electric field intensity's distribution around the nanoparticles could be fine-tuned, thereby adjusting the position and intensity of the SERS hotspots.

THEORETICAL CALCULATIONS

The finite-difference time-domain method (FDTD, Lumerical Solutions, Inc.) software was used to simulate the angle-dependent electric field intensity curve and surface plasmon resonance (SPR) curve under the five-phase WCSPR structure of an SF10 prism (n = 1.79 at 532 nm) with an inner Ag film (n = 0.1293 + 3.1959i at 532 nm), SiO_2 film (n = 1.46 at 532 nm), outer Ag film, and water (n = 1.33 at 532 nm). According to the simulation results, the thinner the outer silver film, the stronger the electric field intensity. However, when the silver film is too thin, it can be difficult to form a continuous silver film. Therefore, we set the thickness of the outer silver film at 5 nm. As shown in Figure 1, the thickness of SiO_2 affects the angle of surface plasmon resonance and the incident angle, which correspond to the maximum electric field intensity. The SPR angle and the incident angle corresponding to the maximum electric field intensity both increase with an increase in the thickness of SiO_2. Moreover, the SPR angle and the incident angle corresponding to the maximum electric field intensity for S-polarization increase faster than those for P-polarization. When the thickness of SiO_2 is 354 nm, the SPR angle for S-polarized light is the same as that for P-polarized light, which is 48.90°. Similarly, when the thickness of SiO_2 is 349 nm, the incident angle corresponding to the maximum electric field intensity of the S-polarized light is the same as that of the P-polarized light, which is 48.77°.

By adjusting the thickness of the SiO_2 film layer, the SPR angles corresponding to P-polarized and S-polarized incident light can be regulated, thereby ensuring that the incident angles corresponding to the maximum electric field intensities of both P-polarized and S-polarized incident light are aligned. This allows for the simultaneous enhancement of SERS signals for both P- and S-polarized incident light. When the thicknesses of the inner silver film, SiO_2 film, and outer silver film are 25, 349, and 5 nm, respectively, the SPR angles for P-polarized and S-polarized incident light are almost equal, measuring 48.83 and 48.80°, respectively. At this point, the incident angle corresponding to the maximum electric field intensity for both P-polarized and S-polarized incident light is 48.77°. At this optimum angle, both P- and S-polarized light can simultaneously enhance the SERS signal. So, we chose to use a five-layer WCSPR structure, which consists of a prism, a 25 nm silver film, a 349 nm SiO_2 film, a 5 nm outer silver film, and a water layer, for both simulation and experimental research in this study. Figure 2a–c illustrate the structure under P-polarization, S-polarization, and 45°-polarization of the incident light, respectively. The SPR curves under different polarization states are shown in Figure 2d, corresponding to P-polarization, S-polarization, and 45°-polarization of the incident light, which have resonance angles of 48.83, 48.80, and 48.80°, respectively. Additionally, Figure 2e shows the angle-dependent surface electric field intensity curves for P-polarization, S-polarization, and 45°-polarization of the incident laser. The maximum electric field intensity enhancements are 59.63, 16.84, and 38.24°, respectively, all corresponding to a common incident angle of 48.77°. Finally, Figure 2f presents the SPR curve and the angle-dependent surface electric field intensity curve under excitation with a 45°-polarization laser.

The FDTD software was also used to simulate the electric field distribution of the WCSPR structure with silver nanoparticles adsorbed, as depicted in Figure 3. Upon exciting the nanoparticles with a P-polarized laser, the electric field on the upper and lower parts increased by approximately 4000

https://doi.org/10.1021/acsomega.3c06740
ACS Omega 2023, 8, 41953−41959

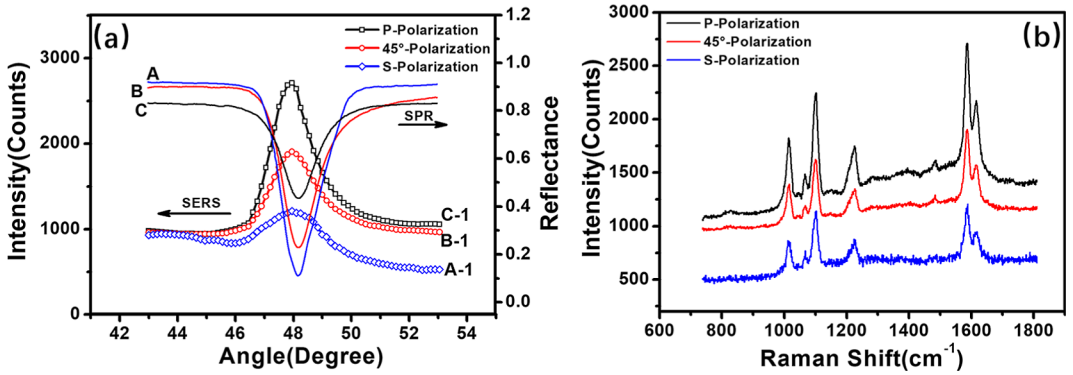

Figure 4. (a) SPR curve (curve A) and SERS intensity profile of angle-dependent SERS excited by S-polarized laser based on the WCSPR structure (curve A-1); SPR curve (curve B) and SERS intensity profile of angle-dependent SERS excited by 45°-polarized laser based on the WCSPR structure (curve B-1); SPR curve (curve C) and SERS intensity profile of angle-dependent SERS excited by S-polarized laser based on the WCSPR structure (curve C-1). All SERS intensity profiles were obtained by plotting the SERS band intensities at 1583 cm^{-1}. The integration time was 1 s (b) SERS spectra obtained in water from the excitation of surface plasmons at a resonance angle of 47.95° based on the WCSPR structure with S-polarization laser excitation (bottom curve), 45°-polarization laser excitation (middle curve), and P-polarization laser excitation (top curve).

times, while the left and right parts were enhanced by approximately 400 times under a S-polarized laser, as shown in Figure 3d,e. When a 45° polarized laser was used, all the parts of the nanoparticle experienced an enhancement in electric fields, with an increase of 5000 times for the upper and lower parts and 500 times for the right and left parts, as displayed in Figure 3f. Thus, the combined nanoparticles and WCSPR structure can result in more SERS hot spots when excited with a 45°-polarized laser. Furthermore, modifying the polarization direction of the incident light can adjust the electric field distribution on the surface of nanoparticles. Supporting Information presents the electric field distribution around the nanoparticles when exposed to different polarizations of the excitation laser.

EXPERIMENTAL METHODS

This study utilized an in-house-built angle-dependent SPR-SERS microspectrometer to simultaneously measure SPR curves and incident angle-dependent SERS spectra. The microspectrometer comprises three main functional parts: an incident light system, an SPR detection system, and an SERS detection system. SERS was excited with a 532 nm laser, and the polarization direction of the laser could be adjusted by using a polarizer and half-wave plate. The incident angle could be tuned via a goniometer. When the 532 nm laser was focused on the Ag film surface, a portion of the incident beam was reflected and collected by the SPR detection system. Simultaneously, the SERS signal of the analytes was captured using the SERS detection system via a microscope with a 20× objective lens under the prism and was further detected by a monochromator (iHR550, Jobin-Yvon Co.) and CCD (Synapse, Jobin-Yvon Co.). The in-house-built angle-dependent SPR-SERS microspectrometer is illustrated in the Supporting Information.

Our study involved the construction of a five-phase WCSPR configuration consisting of a prism/inner silver film/SiO_2 film/outer silver film/water. To create this configuration, SiO_2 and silver films of varying thicknesses were deposited on the bottom of SF10 prisms using vacuum deposition at a pressure of 8.0×10^{-4} Pa. Thermal evaporation was used to deposit the silver film, while the SiO_2 film was coated using the electron beam evaporation method. The thicknesses of the inner silver film, SiO_2 layer, and outer silver film were 25, 349, and 5 nm, respectively. The deposition process was monitored using a thin-film deposition controller (INFICON SQC-310).

For Raman measurements using the WCSPR structure, a 10^{-5} M solution of 4-mercaptopyridine (4-Mpy) was injected into the flow cell and left to incubate for 1 h. Subsequently, water was introduced into the flow cell to wash the silver film surface and eliminate any unabsorbed 4-Mpy molecules. In our design, 4-Mpy molecules were adsorbed onto the Ag films by mercapto groups to form a monolayer that served as the signal emitter. This 4-Mpy monolayer was excited by SPs and emitted SERS signals in an evanescent field. We employed our in-house-built SPR-SERS microspectrometer to simultaneously record the SPR curves and incident angle-dependent SERS spectra of 4-Mpy.[20] The polarization direction of the incident laser could be adjusted by using a polarizer and a half-wave plate.

For Raman measurements using the WCSPR/silver nanoparticle structure, we assembled the silver nanoparticles on the WCSPR structure by injecting the silver colloid and 4-Mpy solution into the flow cell. In our design, the silver nanoparticles were captured by 4-Mpy and immobilized onto the silver film surface. The reaction was maintained for an hour. The silver colloid was prepared using Lee's method, with an average nanoparticle diameter of about 60 nm.[24]

RESULTS AND DISCUSSION

The SPR and SERS signals were measured under different polarization incident light excitations on both the WCSPR configuration and the WCSPR configuration with added silver nanoparticles. As shown in Figure 4a, we obtained the SPR curves and SERS intensity profiles on the WCSPR configuration using S-polarized light, 45°-polarized light, and P-polarized light. First, using the SPR-SERS microspectrometer, we recorded the incident angle-dependent SERS spectra of 4-Mpy (Figure S3 in the Supporting Information) and SPR curve under S-polarization light excitation. Curve A in Figure 4a represents the SPR curve of the WCSPR configuration with an SPR angle of 48.18°. Curve A-1 in Figure 4a shows the spectral intensities (1583 cm^{-1}) plotted against incident angles. The incident angle corresponding to the maximum SERS intensity is 47.95°. The SERS intensity near the resonance angles (i.e., 47.95°) is roughly 3 times stronger than that at nonresonance angles (i.e., 53°). Second, we

https://doi.org/10.1021/acsomega.3c06740
ACS Omega 2023, 8, 41953−41959

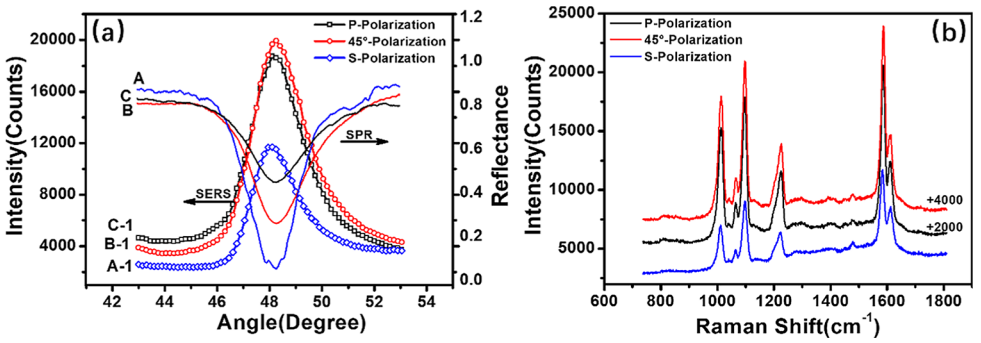

Figure 5. (a) SPR curve (curve A) and intensity profile of angle-dependent SERS excited by S-polarized laser based on the WCSPR/silver-nanoparticle structure (curve A-1); SPR curve (curve B) and intensity profile of angle-dependent SERS excited by 45°-polarized laser based on the WCSPR/silver-nanoparticle structure (curve B-1); SPR curve (curve C) and intensity profile of angle-dependent SERS excited by S-polarized laser based on the WCSPR/silver-nanoparticle structure (curve C-1). All intensity profiles were obtained by plotting the SERS band intensities at 1583 cm^{-1}. The integration time was 1 s. (b) SERS spectra obtained in water from the excitation of surface plasmons at the resonance angle based on the WCSPR/silver nanoparticle structure with S-polarization laser excitation (bottom curve), 45°-polarization laser excitation (top curve), and P-polarization laser excitation (middle curve).

measured the incident angle-dependent SERS spectra (Figure S4 in the Supporting Information) of the 4-Mpy and SPR curves using the SPR-SERS microspectrometer under 45°-polarization incident light excitation. The resonance angle is 48.20° (curve B in Figure 4a), while curve B-1 is the plot of SERS intensities of 4-Mpy at 1583 cm^{-1} vs the incident angles. The incident angle giving the maximum SERS intensity is also 47.95°. The SERS intensity near the resonance angles (i.e., 47.95°) is approximately 3 times stronger than that at nonresonance angles (i.e., 53°). Lastly, under P-polarization light excitation, we measured the SPR curve (curve C in Figure 4a) and the incident angle-dependent SERS spectra of 4-Mpy (Figure S5 in the Supporting Information), with the SPR angle remaining almost the same as the resonance angle of curves B and A at 48.22°. We plotted the incident angle-dependent SERS signals at 1583 cm^{-1} under P-polarization light excitation (curve C-1 in Figure 4a). The maximal SERS spectrum was obtained at an incident angle of 47.95°, which is about 3 times stronger than that at nonresonance angles (i.e., 53°). As shown in Figure 4, the maximally enlarged electromagnetic field led to the highest SERS signals near the SPR angle. With the WCSPR structure, the SERS signal at the SPR resonance angle is the weakest when excited by S-polarized light, becomes stronger at the resonance angle when excited by 45°-polarized light, and is at its strongest when excited by P-polarized light. Figure 4b shows the SERS spectral signals measured with different polarization incident light excitations near the resonance angles (47.95°) at which the SERS intensity was the strongest.

We also obtained the SPR and SERS signals using different polarization incident light excitations on the WCSPR configuration with added silver nanoparticles. Figure 5a displays the SPR curves and SERS intensity versus incident angle under excitation with S-polarized, 45°-polarized, and P-polarized incident light. The incident angle-dependent SERS signals of 4-Mpy on the WCSPR/silver-nanoparticle structure were shown in the Supporting Information (Figures S6–S8). As shown in Figure 5, the highest SERS signals were observed near the SPR angle, where the electromagnetic field was largest. Curve A in Figure 5a represents the SPR curve under S-polarized incident light excitation with an SPR angle of 48.28°. The incident angle corresponding to the maximum SERS intensity is 48.10°. Curve A-1 in Figure 5a is the plot of the spectral intensity (1583 cm^{-1}) against the incident angle under S-polarized incident light excitation. Under 45° polarized incident light, the SPR curve and spectral intensity (1583 cm^{-1}) versus incident angle are shown as curve B and curve B-1 in Figure 5a, respectively, with a SPR angle of 48.28°. The incident angle corresponding to the maximum SERS intensity is 48.10°. For P-polarized incident light, curves C and C-1 in Figure 5a are SPR curves and spectral intensity values (1583 cm^{-1}) versus incident angle, respectively, with an SPR angle of 48.28°. The incident angle giving the maximum SERS intensity is again 48.25°. Figure 5b shows the SERS spectral signals measured with different polarization incident light excitations near the resonance angles, at which the SERS intensity was the strongest (48.10, 48.10, and 48.25° for the S-polarized incident light, 45°-polarized incident light, and P-polarized incident light, respectively).

When excited by P-polarized light on a WCSPR structure, the strongest SERS signal intensity was 1281 counts (removing the background signal). With the addition of nanoparticles, it increased to 14,450 counts, an 11-fold enhancement. Similarly, S-polarized light on the WCSPR structure resulted in a 556 counts signal intensity, which increased to 7090 counts, and also a 13-fold enhancement. When excited by 45°-polarized light on the WCSPR structure, the strongest SERS signal intensity was 922 counts. After adding nanoparticles, it significantly increased to 15,586 counts, which is a 17-fold enhancement. Notably, the SERS signal enhancement was greater under 45°-polarized light excitation compared with P-polarized and S-polarized light excitation. We concluded that P-polarized light only increases the electric field in the upper and lower regions of the nanoparticles, while S-polarized light only increases the electric field in the right and left regions. At 45°-polarized light, the electric field all around the nanoparticles is enhanced, leading to the formation of more hot spots and a better SERS signal boost.

CONCLUSIONS

In summary, a 5-layer WCSPR structure was developed using prism/Ag/SiO_2/Ag/water to enhance Raman scattering. This structure enables both P-polarized and S-polarized incident light to generate an SPR and produces a strong electromagnetic field enhancement at the same SPR angle, which is used to enhance Raman scattering. The thickness of each film layer in the WCSPR structure was adjusted to ensure that the

https://doi.org/10.1021/acsomega.3c06740
ACS Omega 2023, 8, 41953−41959

SPR angle under P-polarized incident light matches the SPR angle under S-polarized incident light, thus enabling both types of incident light to enhance the SERS signal simultaneously. The addition of silver nanoparticles to the WCSPR structure enhanced the electric field intensity of the upper, lower, left, and right parts of the nanoparticles simultaneously when 45°-polarized light was incident, resulting in more hotspots that produce SERS signals comparable to those produced by P-polarized light. It is worth noting that unlike traditional hot spots formed in small gaps, the strongest electric field surrounds the nanoparticles within the WCSPR structure. This facilitates the high-sensitivity SERS detection of compounds and biological macromolecules, such as proteins and DNA, that cannot be placed in traditional gap-type hot spots.

■ ASSOCIATED CONTENT

Supporting Information

The Supporting Information is available free of charge at https://pubs.acs.org/doi/10.1021/acsomega.3c06740.

Simulation of the electric field distribution around the nanoparticles with different polarizations of the excitation laser, angle-dependent SPR-SERS microspectrometer, and incident angle-dependent SERS spectra of 4-Mpy (PDF)

■ AUTHOR INFORMATION

Corresponding Author

Yijia Geng − *State Key Laboratory of Applied Optics, Changchun Institute of Optics, Fine Mechanics and Physics, Chinese Academy of Sciences, Changchun 130033, China; University of Chinese Academy of Sciences, Beijing 100049, China*; Email: gengyijia@ciomp.ac.cn

Authors

Yu Liu − *State Key Laboratory of Applied Optics, Changchun Institute of Optics, Fine Mechanics and Physics, Chinese Academy of Sciences, Changchun 130033, China; University of Chinese Academy of Sciences, Beijing 100049, China;* orcid.org/0000-0002-9815-0060

Jingqiu Liang − *State Key Laboratory of Applied Optics, Changchun Institute of Optics, Fine Mechanics and Physics, Chinese Academy of Sciences, Changchun 130033, China; University of Chinese Academy of Sciences, Beijing 100049, China*

Shuping Xu − *State Key Laboratory of Supramolecular Structure and Materials, Jilin University, Changchun 130012, China;* orcid.org/0000-0002-6216-6175

Complete contact information is available at: https://pubs.acs.org/10.1021/acsomega.3c06740

Funding

Science and Technology Development Project of Jilin Province (nos. 20210201026GX and 20210204188YY). National Natural Science Foundation of China (no. 21603211).

Notes

The authors declare no competing financial interest.

■ ACKNOWLEDGMENTS

Thanks for the support of the ShuGuang Project of the Changchun Institute of Optics, Fine Mechanics and Physics, the Chinese Academy of Sciences, and the Autonomous Fund of the State Key Laboratory of Applied Optics.

■ REFERENCES

(1) Culha, M. Surface-enhanced Raman scattering: an emerging label-free detection and identification technique for proteins. *Appl. Spectrosc.* **2013**, *67*, 355−364.

(2) Lin, S. C.; Ze, H. J.; Zhang, X. G.; Zhang, Y. J.; Song, J.; Zhang, H. M.; Zhong, H. L.; Yang, Z. L.; Yang, C. Y.; Li, J. F.; Zhu, Z. Direct and Simultaneous Identification of Multiple Mitochondrial Reactive Oxygen Species in Living Cells Using a SERS Borrowing Strategy. *Angew. Chem., Int. Ed.* **2022**, *61*, No. e202203511.

(3) Perumal, J.; Wang, Y.; Attia, A. B. E.; Dinish, U. S.; Olivo, M. Towards a point-of-care sers sensor for biomedical and agri-food analysis applications: a review of recent advancements. *Nanoscale* **2021**, *13*, 553−580.

(4) Langer, J.; Jimenez de Aberasturi, D.; Aizpurua, J.; Alvarez-Puebla, R. A.; Auguié, B.; Baumberg, J. J.; Bazan, G. C.; Bell, S. E. J.; Boisen, A.; Brolo, A. G.; et al. Present and future of surface-enhanced Raman scattering. *ACS Nano* **2020**, *14*, 28−117.

(5) Pérez-Jiménez, A. I.; Lyu, D.; Lu, Z. X.; Liu, G. K.; Ren, B. Surface-enhanced Raman spectroscopy: benefits, trade-offs and future developments. *Chem. Sci.* **2020**, *11*, 4563−4577.

(6) Chuang, Y. T.; Cheng, T. Y.; Kao, T. L.; Liao, M. Y. Hollow Au_xCu_{1-x} Alloy Nanoshells for Surface-Enhanced Raman-Based Tracking of Bladder Cancer Cells Followed by Triggerable Secretion Removal. *ACS Appl. Nano Mater.* **2020**, *3*, 7888−7898.

(7) Fan, M.; Andrade, G. F. S.; Brolo, A. G. A review on recent advances in the applications of surface-enhanced Raman scattering in analytical chemistry. *Anal. Chim. Acta* **2020**, *1097*, 1−29.

(8) Wang, X.; Huang, S. C.; Hu, S.; Yan, S.; Ren, B. Fundamental understanding and applications of plasmon- enhanced Raman spectroscopy. *Nat. Rev. Phys.* **2020**, *2*, 253−271.

(9) Ivanov, V. G.; Vlakhov, E. S.; Stan, G. E. Surface-enhanced Raman scattering activity of niobiu surface after irradiation with femtosecond laser pulses. *J. Appl. Phys.* **2015**, *118*, 203104.

(10) Saito, K.; McGehee, K.; Norikane, Y. Size-controlled synthesis of cyclodextrin-capped gold nanoparticles for molecular recognition using surface-enhanced Raman scattering. *Nanoscale Adv.* **2021**, *3*, 3272−3278.

(11) Zhang, J. H.; Mai, X. M.; Hong, X. M.; Chen, Y. Z.; Li, X. J. Optical fiber SPR biosensor with a solid-phase enzymatic reaction device for glucose detection. *Sens. Actuators, B* **2022**, *366*, 131984.

(12) Huang, X. X.; Wang, H. J.; Yang, J. L.; Yue, M. F.; Wang, Y. H.; Zhang, H.; Li, J. F. Direct S−H Evidence Revealing the Photoelectrocatalytic Hydrogen Evolution Reaction Mechanism on CdS Using Surface-Enhanced Raman Spectroscopy. *J. Phys. Chem. Lett.* **2023**, *14*, 4026−4032.

(13) Yu, H.; Yang, Z. L.; Fu, S. Y.; Zhang, Y. J.; Panneerselvamc, R.; Li, B. Q.; Zhang, L.; Chen, Z. H.; Wang, X.; Li, J. F. Intelligent Convolution Neural Network-Assisted Sers to Realize Highly Accurate Identification of Six Pathogenic Vibrio. *Chem. Commun.* **2023**, *59*, 5779−5782.

(14) Ding, S. Y.; You, E. M.; Tian, Z. Q.; Moskovits, M. Electromagnetic theories of surface-enhanced Raman spectroscopy. *Chem. Soc. Rev.* **2017**, *46*, 4042−4076.

(15) Zhang, J. X.; Zhang, L. D. Nanostructures for surface plasmons. *Adv. Opt. Photon* **2012**, *4*, 157−321.

(16) Awada, C.; Dab, C.; Grimaldi, M. G.; Alshoaibi, A.; Ruffino, F. High optical enhancement in au/ag alloys and porous au using surface-enhanced raman spectroscopy technique. *Sci. Rep.* **2021**, *11*, 4714.

(17) Krajczewski, J.; Michalowska, A.; Ctvrtlik, R.; Nožka, L.; Tomáštík, J.; Václavek, L.; Turczyniak-Surdacka, S.; Bieńskowski, K.; Solarska, R. The battle for the future of SERS−TiN vs Au thin films with the same morphology. *Appl. Surf. Sci.* **2023**, *618*, 156703.

(18) Wang, Z. L.; Zervas, M.; Bartlett, P. N.; Wilkinson, J. S. Surface and waveguide collection of Raman emission in waveguide-enhanced Raman spectroscopy. *Opt. Lett.* **2016**, *41*, 4146−4149.

(19) Wan, X. M.; Gao, R.; Lu, D. F.; Qi, Z. M. Self-referenced directional enhanced Raman scattering using plasmon waveguide resonance for surface and bulk sensing. *Appl. Phys. Lett.* **2018**, *112* (4), 1−5.
(20) Liu, Y.; Xu, S. P.; Tang, B.; Wang, Y.; Zhou, J.; Zheng, X. L.; Zhao, B.; Xu, W. Q. Simultaneous Measurement of Surface Plasmon Resonance and Surface-Enhanced Raman Scattering. *Rev. Sci. Instrum.* **2010**, *81*, 036105−036107.
(21) Pettinger, B.; Tadjeddine, A.; Kolb, D. M. Enhancement in Raman intensity by use of surface plasmons. *Chem. Phys. Lett.* **1979**, *66*, 544−548.
(22) Simon, H. J.; Mitchell, D. E.; Watson, J. G. Optical Second-Harmonic Generation with Surface Plasmons in Silver Films. *Phys. Rev. Lett.* **1974**, *33*, 1531−1534.
(23) Tsang, J. C.; Kirtley, J. R.; Bradley, J. A. Surface-Enhanced Raman Spectroscopy and Surface Plasmons. *Phys. Rev. Lett.* **1979**, *43*, 772−775.
(24) Wang, L.; Geng, Y. J.; Zhang, S. D.; Liang, J. Q.; Xu, S. P.; Liu, Y. Propagating and Localized Surface Plasmon Co-Enhanced Raman Scattering Based on a Waveguide Coupling Surface Plasmon Resonance Structure. *J. Phys. Chem. C* **2023**, *127*, 4188−4194.
(25) Chen, C.; Liu, Z. W.; Cai, C.; Qi, Z. M. Facile fabrication of nanoporous gold films for surface plasmon resonance (SPR) sensing and SPR-based SERS. *J. Mater. Chem. C* **2021**, *9*, 6815−6822.
(26) McKee, K. J.; Meyer, M. W.; Smith, E. A. Near IR Scanning Angle Total Internal Reflection Raman Spectroscopy at Smooth Gold Films. *Anal. Chem.* **2012**, *84*, 4300−4306.
(27) De Leon, I.; Berini, P. Amplification of long-range surface plasmons by a dipolar gain medium. *Nat. Photonics* **2010**, *4*, 382−387.
(28) Konopsky, V. N. Long-range surface plasmons on duplex metal nanolayers. *Photonics Nanostruct.* **2020**, *39*, 100788.
(29) Liu, Y.; Xu, S. P.; Xuyang, X.; Zhao, B.; Xu, W. Q. Long-Range Surface Plasmon Field-Enhanced Raman Scattering Spectroscopy Based on Evanescent Field Excitation. *J. Phys. Chem. Lett.* **2011**, *2*, 2218−2222.
(30) Tian, Y.; Wang, H. L.; Xu, W. Q.; Liu, Y.; Xu, S. P. Waveguide-coupled localized surface plasmon resonance for surface-enhanced Raman scattering: Antenna array as emitters. *Sens. Actuators, B* **2019**, *280*, 144−150.
(31) McKee, K. J.; Meyer, M. W.; Smith, E. A. Plasmon Waveguide Resonance Raman Spectroscopy. *Anal. Chem.* **2012**, *84*, 9049−9055.
(32) Zhang, H. T.; Geng, Y. J.; Xu, S. P.; Xu, W. Q.; Tian, Y.; Yu, J.; Deng, W. Y.; Yu, B.; Liu, Y. Surface Plasmon Field-Enhanced Raman Scattering Based on Evanescent Field Excitation of Waveguide-Coupled Surface Plasmon Resonance Configuration. *J. Phys. Chem. Lett.* **2020**, *124*, 1640−1645.
(33) Joshi, A.; Manjuladevi, V.; Kumar Gupta, R. Facile layered structure of sensing chip of a prism−based surface plasmon resonance device. *Mater. Today: Proc.* **2022**, *63*, 647−652.
(34) Tian, Y.; Wang, H. L.; Geng, Y. J.; Cong, L. l.; Liu, Y.; Xu, W. Q.; Xu, S. P. Boosting a sub-10nm nanogap array by plasmon-triggered waveguide resonance. *Photon. Res.* **2020**, *8*, 1850−1856.
(35) Gu, Y. J.; Xu, S. P.; Li, H. B.; Wang, S.; Cong, M.; Lombardi, J. R.; Xu, W. Q. Waveguide-Enhanced Surface Plasmons for Ultra-sensitive SERS Detection. *J. Phys. Chem. Lett.* **2013**, *4*, 3153−3157.

https://doi.org/10.1021/acsomega.3c06740
ACS Omega 2023, 8, 41953−41959